Dalton Transactions

PAPER

View Article Online
View Journal | View Issue

Cite this: *Dalton Trans.*, 2015, **44**, 16923

Synthesis of colloidal InSb nanocrystals *via in situ* activation of $InCl_3$†

Sudarsan Tamang,[a,b] Kyungnam Kim,[a] Hyekyoung Choi,[a,c] Youngsik Kim[a,c] and Sohee Jeong*[a,c]

Received 9th June 2015,
Accepted 25th August 2015

DOI: 10.1039/c5dt02181b

www.rsc.org/dalton

Indium antimonide (InSb), a narrow band gap III–V semiconductor is a promising infrared-active material for various optoelectronic applications. Synthetic challenge of colloidal InSb nanocrystals (NCs) lies in the limited choice of precursors. Only a few successful synthetic schemes involving highly toxic stibine (SbH_3) or air- and moisture-sensitive metal silylamides ($In[N(Si\text{-}(Me)_3)_2]_3$ or $Sb[N(Si\text{-}(Me)_3)_2]_3$) as the precursor have been reported. We found that commercially available precursors $InCl_3$ and $Sb[NMe_2]_3$ directly form highly crystalline colloidal InSb nanocrystals in the presence of a base such as $LiN(SiMe_3)_2$ or *n*BuLi. The mean size of the particles can be controlled by simply changing the activating base. This approach offers a one-pot synthesis of InSb NCs from readily available chemicals without the use of complex organometallic precursors.

Introduction

There is a significant technological importance in synthesizing semiconductor nanocrystals (NCs) in the colloidal form. The solution processed colloidal NCs facilitate cost effective surface modification and device fabrication techniques.[1–7] InSb is one of the important members of the III–V semiconductor. High electron mobility (bulk InSb value: 78 000 $cm^2\ V^{-1}\ s^{-1}$), a narrow band gap (*e.g.* bulk = 0.17 eV), a large exciton Bohr radius (a_B, calculated ~60 nm), and a high static dielectric constant (ε = 17.88) are some of the exciting properties of the InSb semiconductor.[8,9] In addition, InSb has a relatively low melting temperature (~527 °C) and it has been proposed that in the colloidal form these NCs could be directly used as single source soluble precursors for developing low cost films by annealing at near melting temperatures.[10] Despite their tremendous potential as solution-processable infrared (IR) active materials, few reports exist in the literature as far as syntheses of colloidal InSb nanocrystals are concerned.[10–12] One of the major challenges in the synthesis of colloidal InSb nanocrystals is the lack of appropriate precursors. Precursor reactivity has to be carefully controlled for facile synthesis of InSb NCs. Wells' dehalosilylation reaction[13,14] which has been the cornerstone for InP and InAs syntheses, has yielded little success in the synthesis of InSb NCs.[15] The reason for this ineffectiveness is the decreased stability of $(TMS)_3Sb$ compared to $(TMS)_3P$ or $(TMS)_3As$ due to the increase in atomic radii from P to Sb. Another potential precursor is SbH_3 gas.[11] However, its toxicity restricts its widespread use in the synthesis of colloidal InSb NCs. Recently, silylamides of indium and antimony have been explored to obtain InSb NCs.[10,12] These silylamides containing polar M–N bonds are commonly used in the syntheses of metal and metalloid nanoparticles (NPs).[16] As far as the use of silylamides in the synthesis of InSb is concerned, two recently published articles deserve a special attention. Liu *et al.* reported the synthesis of colloidal InSb NCs using tris(dimethylsilyl)-amino antimonide as the antimony precursor.[10] The reaction between tris(dimethylsilyl)amino antimonide and indium chloride in the presence of a reducing agent, lithium triethylborohydride, yields InSb NCs. These NCs upon rigorous and extensive size selective precipitation deliver InSb quantum dots exhibiting size dependent optical properties. More recently Yarema *et al.*[12] synthesized InSb NCs by directly reacting tris(dimethylsilyl)amino indium with a commercially available antimony precursor, tris(dimethylamido) antimony, $Sb[NMe_2]_3$.[17] However, one major drawback of using silylamide precursors is that, many of them including indium and antimony silylamide precursors are commercially unavailable; they need to be synthesized and their synthesis typically involves lengthy reaction times and rigorous purification steps. For example, to synthesize $In[N(SiMe_3)_2]_3$, the reactants, $InCl_3$ and $LiN(SiMe_3)_2$ are refluxed for 24 h. The product is then purified by recrystallizing from diethyl ether at −10 °C multiple times.

[a]*Nanomechanical Systems Research Division, Korea Institute of Machinery and Materials, Daejeon 305-343, Korea. E-mail: sjeong@kimm.re.kr*
[b]*Department of Chemistry, Sikkim University, 737102 Sikkim, India*
[c]*Department of Nanomechatronics, Korea University of Science and Technology (UST), Daejeon 305-350, Korea*

†Electronic supplementary information (ESI) available: Fig. S1–S3 and Table S1. See DOI: 10.1039/c5dt02181b

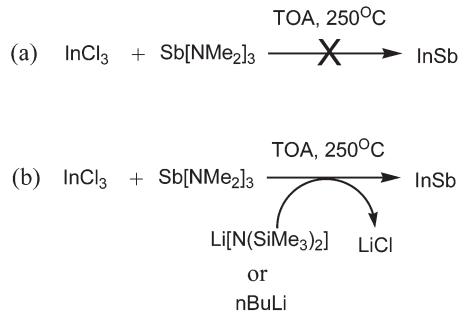

Scheme 1 InSb synthesis using $InCl_3$ and $Sb[NMe_2]_3$ as precursors in trioctylamine (TOA) at 250 °C. (a) No InSb NCs form without the base. (b) In the presence of the base, $Li[N(SiMe_3)_2]$ or *n*BuLi, reaction yields InSb NCs.

In addition, the metal silylamides are extremely air- and moisture-sensitive.[12,18] Here, we demonstrate a simple strategy for the synthesis of colloidal InSb NCs without the use of pre-synthesized silylamides. We initially attempted to synthesize InSb NCs using $InCl_3$ as the indium source and $Sb[NMe_2]_3$ as the antimony precursor. While they did not form InSb NCs under typical colloidal synthetic conditions, in the presence of a strong base such as $LiN(SiMe_3)_2$ or *n*-BuLi the same reaction gave the desired product (Scheme 1). This simple approach thus resulted in the formation of highly crystalline InSb NCs within a few minutes and also eliminated the use of sensitive organometallic indium precursors or cumbersomely synthesized silylamides. Further, based on a series of control experiments and XRD spectral analysis of the products, plausible mechanistic pathways for the formation of InSb NCs in the presence of a base have been proposed. The base reacts rapidly with $InCl_3$ and *in situ* generates reactive indium species which in the presence of $Sb[NMe_2]_3$ at high temperature trigger nucleation and growth of InSb.

Experimental

Chemicals used

Indium(III) chloride ($InCl_3$, 99.99%); lithium hexamethyldisilazide, ($LiN(SiMe_3)_2$, 97%); tris(dimethylamino)antimony, $Sb(NMe_2)_3$, 99.99%; *n*-butyl lithium, (*n*BuLi, 1.6 M in hexane); trioctylamine (TOA, 98%); oleic acid (≥99%); tetrachloroethylene (anhydrous >99%); and lithium triethylborohydride (superhydride, 1.0 M in THF). Unless otherwise stated, all chemicals were purchased from Sigma-Aldrich and were used as supplied. TOA was degassed at 150 °C for 2 h under vacuum (~0.5 mbar) prior to use.

Synthesis of InSb NCs using $Li[N(SiMe_3)_2]$

0.125 mmol of $InCl_3$ was mixed with 10 mL of degassed TOA in a 50 mL round bottomed flask and the mixture was degassed at 120 °C for 1 h under vacuum (~0.5 mbar). 0.18–0.37 mmol of $Li[N(SiMe_3)_2]$ and 0.0625 mmol of $Sb[NMe_2]_3$ were dissolved in 3 mL anhydrous TOA solution in a glove box (solution B). Solution B was rapidly injected into solution A at 250 °C. The temperature dropped to 220 °C. Heating was continued for 5–60 minutes. To quench the reaction 5 mL anhydrous hexane solution was added and when the temperature dropped below 150 °C, the reaction flask was immersed in a cold water bath. 10 mL of crude solution was mixed with 10 mL hexane : acetone (1 : 1) solvent and purified using centrifugation (6000 rpm, 3 minutes, 3 rounds). The pellet was dispersed in 2% oleic acid solution in tetrachloroethylene (TCE).

Synthesis of InSb NCs using *n*BuLi

0.125 mmol of $InCl_3$ was mixed with 10 mL of degassed TOA in a 50 mL round bottomed flask and the mixture was degassed at 120 °C for 1 h under vacuum (~0.5 mbar). The mixture was then backfilled with N_2 gas and heated to 250 °C. 150 μL of *n*BuLi (0.37 mmol) solution was rapidly injected into $InCl_3$ solution in TOA at 250 °C. This is immediately (within 30 seconds) followed by injection of 12.5 μL $Sb[NMe_2]_3$ (0.0625 mmol) dissolved in 3 mL anhydrous TOA solution in the glove box. The temperature dropped to 230 °C. Heating was continued for 5–10 minutes.

Synthesis of InSb NCs using $LiBHEt_3$

0.125 mmol of $InCl_3$ was mixed with 10 mL of degassed TOA in a 50 mL round bottomed flask and the mixture was degassed at 120 °C for 1 h under vacuum (~0.5 mbar). The mixture was then purged with N_2 gas and heated to 250 °C. 375 μL of $LiBHEt_3$ (0.37 mmol) solution was rapidly injected into $InCl_3$ solution in TOA at 250 °C. After 1 minute 12.5 μL of $Sb[NMe_2]_3$ (0.0625 mmol) dissolved in 3 mL anhydrous TOA solution in the glove box is injected into the reaction mixture. The temperature dropped to 230 °C. Heating was continued for 5–10 minutes.

Characterization

X-ray diffraction patterns were obtained using a PanAlytical (EMPYREAN) diffractometer (Cu source). XRD samples were prepared by drop casting a concentrated solution of NCs (capped with TOA) in anhydrous hexane onto a glass substrate. Transmission electron microscopy (TEM) images and electron diffraction patterns were acquired using a Tecnai F30 Super-Twin TEM microscope operated at 300 keV. The NCs dispersed in TCE containing 2% oleic acid were diluted with hexane and drop casted on a carbon coated Cu grid; UV/Vis/NIR absorption spectra were collected using a Shimadzu UV/Vis/NIR 3600 spectrometer. The NCs dispersed in TCE were used for the absorption measurement; X-ray photoemission (XPS) spectra were measured in PHI Quantera-II surface analysis equipment using an Al monochromator (1486.6 eV). The InSb NCs dispersed in hexane (capped with TOA) were used for XPS measurements. A thin film of NCs was deposited on Si substrates in a glove box. Before deposition, the Si wafers were cleaned using acetone, isopropyl alcohol, and deionized water in a sonication bath. All XPS spectra were fitted with Voigt

functions with a fixed ratio of Lorentzian and Gaussian functions (20 : 80).[19] Other constraints used are In 3d spin–orbit split of 7.54 eV and Sb 3d spin–orbit split of 9.34 eV. WIN95/98 XPSPEAK version 4.1 was used for fitting. Proton nuclear magnetic resonance (^{1}H NMR) was performed using a 600 MHz Bruker NMR using chloroform-*d* as the solvent.

Results and discussion

The effect of $LiN(SiMe_3)_2$ on the reaction between $InCl_3$ and $Sb[NMe_2]_3$ is demonstrated in Fig. 1. Without the $LiN(SiMe_3)_2$, injection of $Sb[NMe_2]_3$ into $InCl_3$ solution in TOA at elevated temperature yields metallic antimony crystals (blue spectrum, Fig. 1a). However, when $Sb[NMe_2]_3$ was injected together with $LiN(SiMe_3)_2$ into the $InCl_3$ solution, colloidal zinc blende InSb NCs were formed (Fig. 1a, black spectra). In a typical synthesis, a weakly coordinating solvent TOA containing $InCl_3$ was heated to 250 °C and a solution containing a mixture of $Sb[NMe_2]_3$ and $LiN(SiMe_3)_2$ in TOA was rapidly injected into it. Even when the reaction was quickly quenched at 1 minute, the XRD pattern obtained from the product showed the signatures of InSb along with that of metallic Sb, while after 5 minutes, the Sb signature disappeared or diminished and evolution of zinc blende InSb signatures was noted as a function of reaction time. Increasing the reaction time to 10, 30 and 60 minutes resulted in sharper XRD peaks indicating the increase in the crystallite size. Fig. 1b presents the change of crystallite size with growth time. Pure zinc blende InSb NCs were obtained by maintaining the In : Sb precursor ratio about 1 : 0.5. Typically, the molar concentration of the base was 1.5 to 3 times the $InCl_3$ concentration. Fig. 1(c) depicts the XRD patterns of the products synthesized at different injection and growth temperatures. The typical injection and growth temperatures were 250 °C and 230 °C respectively. At the injection temperature lower than 250 °C the product invariably showed poor crystallinity. For example, the XRD spectrum of the particles synthesized with injection at 200 °C and growth at 150 °C was featureless indicative of amorphous particles. Similarly, the red spectrum represents the NCs synthesized by injecting precursors at 250 °C and grown at 200 °C for 15 minutes. From these observations, it was evident that the base $LiN(SiMe_3)_2$ was crucial in the formation of InSb NCs from $Sb[NMe_2]_3$ and $InCl_3$ in TOA. To further understand the mechanistic pathways, we conducted a series of experiments as shown in Scheme 2 and monitored the crystal formation using XRD. In the absence of the Sb precursor, when $LiN(SiMe_3)_2$ was injected into a solution of $InCl_3$ in TOA at 250 °C (Scheme 2, route A1), the color of the reaction mixture first changed to bright yellow and then immediately to dark grey within 2 minutes. After 5 minutes, the reaction was stopped and the isolated product was analyzed by XRD. Metallic indium was detected as shown in Fig. 2a. $LiN(SiMe_3)_2$ is known to react with a wide range of metal halides, *via* a metathesis reaction, to form M–N bonded compound, $In[N(SiMe_3)_2]_3$.[12,19] This silylamide is also known to decompose to metallic indium within minutes at high temperature.[20] Based on the literature reports together with the detection of metallic indium in XRD in our control experiment, we propose that the formation of InSb proceeds *via* formation of In–N species 1 (Scheme 1) *in situ*. The high reaction temperature may be the key to formation of $In[N(SiMe_3)_2]_{3-x}Cl_x$ *in situ* which either subsequently decomposes to metallic indium in the absence of the antimony precursor or forms InSb in the presence of the same. $LiN(SiMe_3)_2$ is a strong nucleophilic base ($pK_a \sim 30$) and reacts with protic reagents and solvents.[21,22] The interaction

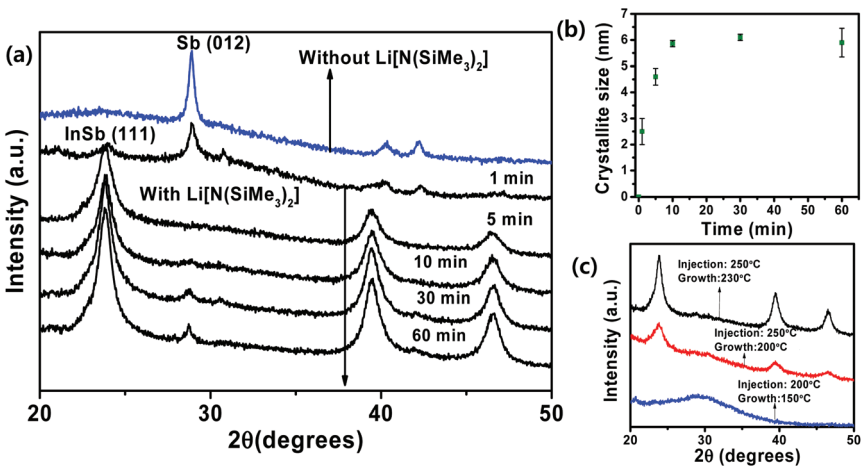

Fig. 1 Evolution of crystalline InSb NCs. (a) XRD spectrum of the product obtained from reaction between $InCl_3$ and $Sb[NMe_2]_3$ without the base, $Li[N(SiMe_3)_2]$ (blue). $InCl_3$ reacts with $Sb[NMe_2]_3$ in the presence of $Li[N(SiMe_3)_2]$ (black) to form InSb. Crystallite size increases as the growth time increases from 1 min to 60 min. (b) The mean crystallite size calculated using the Scherrer equation is plotted as the growth time varies. The error bar indicates the standard deviation of the size calculated from three different XRD peaks (*viz.*, 111, 022, 113) of the same spectrum. (c) Comparison of XRD spectra of InSb NCs synthesized at growth temperatures 230 °C (black), 200 °C (red) and 150 °C (blue), respectively. The injection temperature is 250 °C for first two spectra (black and red) and 200 °C for the last spectrum (blue).

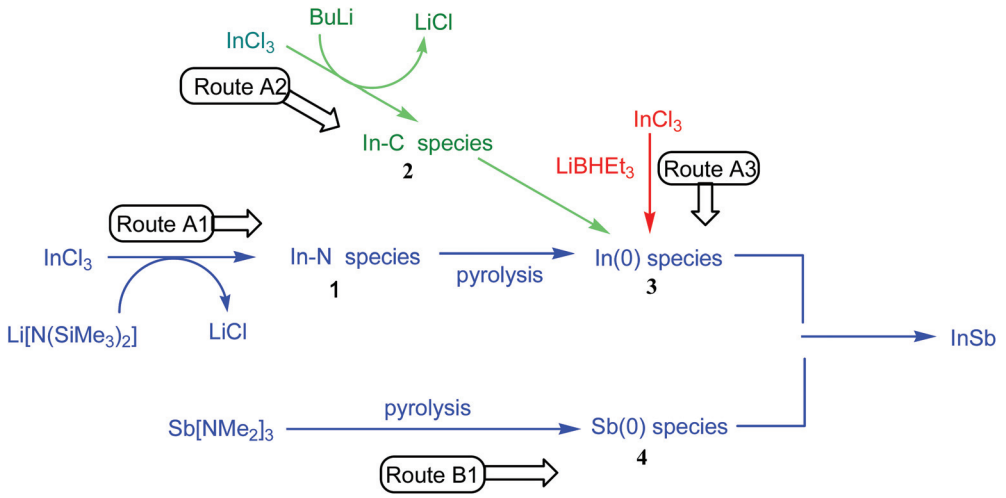

Scheme 2 Formation of InSb by various routes.

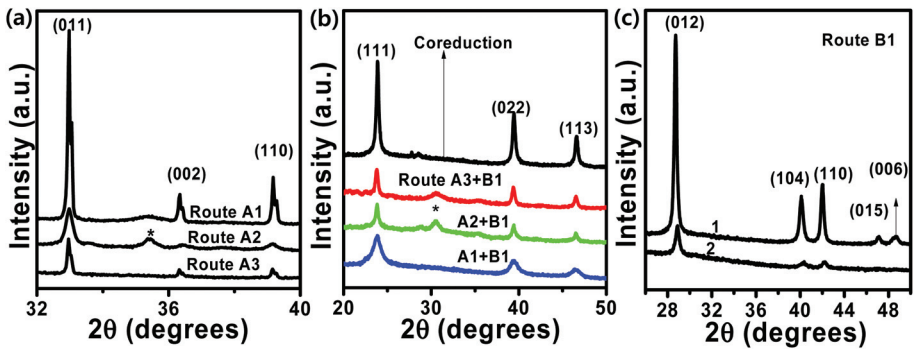

Fig. 2 (a) XRD spectra of metallic indium obtained from various routes, A1, A2 and A3, respectively described in Scheme 2. (b) XRD spectra of InSb NCs obtained from various routes described in Scheme 1. Route A1 + B1 involves the base $LiN(SiMe_3)_2$, while A2 + B1 and A3 + B1 involve *n*BuLi and $LiBHEt_3$ respectively. The InSb NCs synthesized by using different bases have been compared with the particles obtained by co-reduction of In(III) and Sb(III) salts by $LiBHEt_3$. * denotes an impurity peak from LiCl. (c) XRD spectra of metallic indium obtained from various routes (A1, A2 and A3) described in Scheme 2. (c) XRD spectra of antimony obtained from pyrolysis of $Sb[NMe_2]_3$ in TOA at 250 °C. Both in the presence (2) of $InCl_3$ and in the absence (1) of $InCl_3$ pyrolysis of $Sb[NMe_2]_3$ yields antimony. Full range (2θ: 20–80) spectra are provided in the ESI (Fig. S1–S3†).

between $LiN(SiMe_3)_2$ and the solvent like oleylamine is well documented in the synthesis of various metal, metalloid and alloy nanocrystals.[22] We can rule out the side reaction between the solvent and $LiN(SiMe_3)_2$ as in our case the solvent (TOA) being a tertiary amine does not possess acidic hydrogen. We replaced $LiN(SiMe_3)_2$ with a stronger base, *n*BuLi ($pK_a \sim 50$) to further understand the possible reaction pathways (Fig. 2). Like $LiN(SiMe_3)_2$, *n*BuLi is also capable of undergoing a metathesis reaction with $InCl_3$ to form reactive, In–C species 2, which undergoes pyrolysis (Scheme 2, route A2). When *n*BuLi was injected along with $Sb[NMe_2]_3$ to $InCl_3$ solution in TOA, the solution immediately turned black. The XRD pattern of the precipitate confirmed the formation of zinc blende InSb NCs (Fig. 2). The injection of *n*BuLi solution alone into (Scheme 2, route A2) TOA at 250 °C gave metallic indium (Fig. 2, route A2), similar to the results obtained with $LiN(SiMe_3)_2$ (Fig. 2, route A1). The mean crystallite size of the InSb NCs synthesized using *n*BuLi (Fig. 2b), was much larger (~20 nm) than those obtained with $LiN(SiMe_3)_2$ (~5 nm). The *n*BuLi being a stronger base than $LiN(SiMe_3)_2$ ($pK_a \sim 50$ *vs.* $pK_a \sim 30$), the rate of formation of species 2 is expected to be faster than the formation of species 1. In addition, the alkyl indium compounds are chemically unstable at higher temperatures[23] and are known to react uncontrollably with $Sb[NMe_2]_3$.[12] Next, we replaced the base (*viz.*, *n*BuLi or $LiN(SiMe_3)_2$) with $LiBHEt_3$ which is a powerful reducing agent and is expected to directly form In(0) *in situ* (Scheme 2, route A3). The formation of InSb NCs was still observed (Fig. 2). This result strongly supports the formation of InSb in the presence of $LiN(SiMe_3)_2$ and *n*BuLi *via* In(0) species 3. $Sb[NMe_2]_3$ is commonly employed as the Sb-precursor in chemical vapour deposition of epitaxial InSb.[17] Pyrolysis of $Sb[NMe_2]_3$ has been thoroughly investigated by Jensen and coworkers. Various nitrogen containing products such as methylmethyleneimine, dimethyl amine and

methyleneimine are known to form.[24] Although we did not detect these low boiling byproducts in the NMR spectrum of the as-synthesized InSb NCs, the heating of $Sb[NMe_2]_3$ alone in TOA at high temperature resulted in the formation of antimony (Fig. 2C) indicating that $Sb[NMe_2]_3$ undergoes thermal decomposition in TOA to generate Sb(0). Various products obtained from routes outlined in Scheme 2 are presented in Table S1 (ESI†). In the absence of the Sb precursor, routes A1, A2 and A3 all led to the formation of metallic indium (Fig. 2a) while in the absence of an activator and/or an indium precursor route B1 led to the formation of antimony (Fig. 2c). Combinations of A1 + B1, A2 + B1 and A3 + B1 routes all yielded InSb NCs albeit of different crystallite sizes (Fig. 2b). Based on these results, we conclude that the formation of InSb takes place *via* In(0) and Sb(0) as suggested previously.[10] Liu *et al.* have shown that the reaction between $Sb[N(SiMe_3)_2]_3$ and $InCl_3$ in the presence of a $LiBHEt_3$ yields InSb NCs *via* reactive In(0) and Sb(0) species. $LiEt_3BH$ is a strong reducing agent and simultaneously reduces (co-reduction) both In and Sb precursors to form InSb NCs. In our study, we further revealed that the crystallite size of the NCs can be controlled by using different bases capable of undergoing salt metathesis reaction with $InCl_3$. Comparison of the XRD spectra of InSb NCs synthesized using three different molecules, $LiN(SiMe_3)_2$, *n*BuLi, and $LiBHEt_3$, is provided in Fig. 2b. The crystallite sizes were calculated using the Scherrer equation for NCs synthesized with three different bases namely, $LiN(SiMe_3)_2$, *n*BuLi, and $LiBHEt_3$ are 4.63 ± 0.32, 17.96 ± 2.98 and 20.73 ± 0.75 nm, respectively. TEM showed that the mean size of the InSb NCs synthesized using $LiN(SiMe_3)_2$ is 7.2 nm with size dispersion of ~20% (Fig. 3d and e). A slight difference between crystallite size obtained from XRD and particle size obtained from TEM is expected. Larger sized agglomerated NCs (>20 nm) with particle size dispersion of 30–40% were obtained with both *n*BuLi and $LiBHEt_3$. The InSb NCs synthesized by using different bases have been compared with the InSb crystals obtained directly by the co-reduction of In(III) and Sb(III) salts with $LiBHEt_3$.[25]

Synthesized InSb NCs were well dispersed in non-polar solvents like hexane, chloroform, and tetrachloroethylene in the presence of a small amount of oleic acid (~2%). Oleic acid replaces the weakly coordinating TOA and provides greater colloidal stability.[10,12] A well-defined excitonic band was not observed in the UV-Vis-NIR absorption spectrum (Fig. 3(a)). Excessive size selective precipitation might be required as described previously.[10] Because of the highly oxophilic nature of both indium (bond energy, In–O 360 kJ mol^{-1}) and antimony (Sb–O 372 kJ mol^{-1}),[26] InSb is prone to oxidation. Mild room temperature surface oxidation has been commonly observed in InSb samples.[11,12,27] As synthesized InSb NCs capped with TOA were characterized with XPS as shown in Fig. 3(c). The XPS spectrum of the In 3d core level can be deconvoluted into InSb (In $3d_{5/2}$ 444.3 eV), In-ligand (In $3d_{5/2}$ 445.29 eV) and a small In-oxide (In $3d_{5/2}$ 446.2 eV) peak. The presence of a chemically shifted In-ligand signature in XPS is also supported by the NMR data (Fig. 3b). Strong interactions

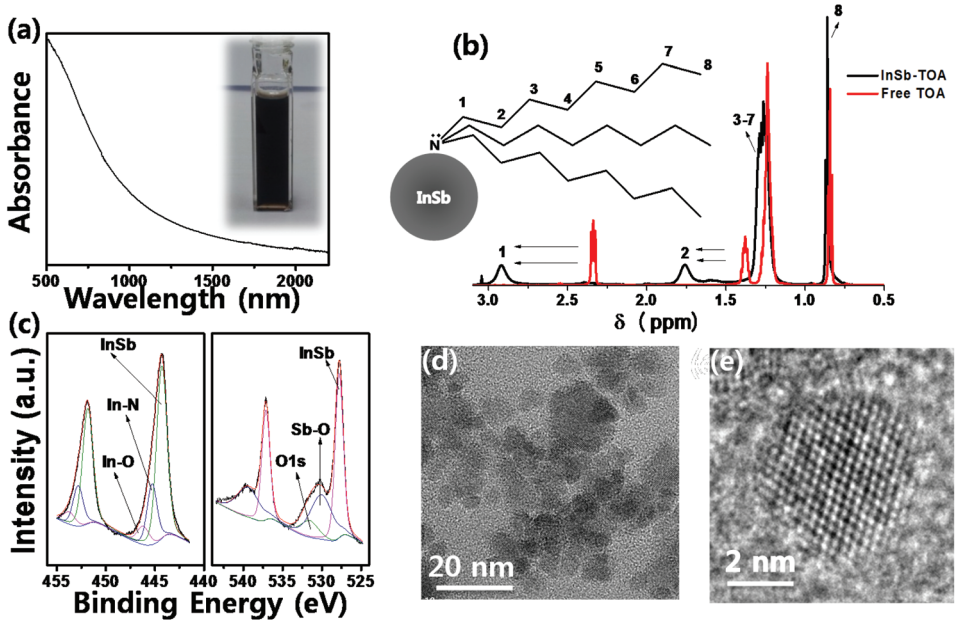

Fig. 3 Characterization of InSb NCs synthesized in the presence of $LiN(SiMe_3)_2$ at reaction time 5 minutes. (a) UV-Vis-NIR absorption of colloidal InSb NCs dispersed in tetrachloroethylene (TCE) in the presence of oleic acid (2%). Inset shows the colloidal solution of InSb NCs in TCE. (b) ^1H NMR spectra of the bound TOA (black) on InSb NCs and free TOA (red). (c) XPS spectra of In 3d (left panel) and Sb 3d (right panel) doublet pairs. Deconvolution is based on indium and antimony species in different chemical environments *viz.*, InSb, In bonded to N of the ligand and In–O or Sb–O which results from mild surface oxidation. O 1s peak overlaps with Sb 3d. (d) Low resolution TEM image NCs. (e) High resolution TEM image of a single InSb particle.

between the nitrogen atom of TOA and the NCs are clearly evident in the NMR spectra of the InSb NCs coated with TOA (Fig. 3b). Not only are the proton signals broad but also they are chemically shifted downfield. For example, a chemical shift of about 0.6 ppm was observed for protons on the carbon-1 atom. Progressively smaller chemical shifts for higher protons (carbon-2, -3, -4 *etc*.) were observed indicative of the inductive effect. The presence of surface oxides was also evident in Sb 3d core level spectra. Besides InSb (Sb $3d_{5/2}$ 527.8 eV), the signals from Sb-oxide (Sb $3d_{5/2}$ 530 eV) are clearly visible. The O 1s signal overlaps with Sb 3d and is assigned at 531.5 eV. The presence of oxides of both In and Sb in the InSb sample is consistent with the literature reports.[27] The TEM (Fig. 3d) image shows the presence of sub-10 nm InSb NCs. Fig. 3e denotes a representative single InSb particle. The *d*-spacing calculated from different particles in HRTEM confirmed the zinc blende structure (space group $f\bar{4}3m$) with a lattice parameter of 0.647 nm at room temperature.

Conclusion

Colloidal InSb NCs were prepared by using commercially available $InCl_3$ and $Sb[NMe_2]_3$ as In and Sb sources respectively. The presence of a strong base such as $LiN(SiMe_3)_2$ or *n*BuLi or $LiBHEt_3$ was crucial for obtaining highly crystalline InSb NCs as well controlling the size of the particle. The role of the base is to convert $InCl_3$ into more reactive In–C or In–N species *via* an *in situ* salt metathesis reaction. This approach offers a single pot method to generate InSb NCs using commercially available reagents and avoids the use of sensitive organometallic indium precursors or cumbersomely synthesized silylamides. Various other potential bases and reducing agents, solvent systems, and reaction conditions could be further investigated to achieve greater control over size and shape of the IR active InSb NCs.

Acknowledgements

This work was supported by the Global Frontier R&D program by the Center for Multiscale Energy Systems (2011-0031566) and the Global R&D program (1415134409). ST acknowledges Sikkim University for sanctioning study leave to carry out this research work in Korea.

References

1 D. V. Talapin, J. S. Lee and M. V. Kovalenko, *Chem. Rev.*, 2010, **110**, 389–458.
2 J. Puthussery, S. Seefeld, N. Berry, M. Gibbs and M. Law, *J. Am. Chem. Soc.*, 2011, **133**, 716–719.
3 I. J. Kramer and E. H. Sargent, *Chem. Rev.*, 2014, **114**, 863–882.
4 V. Wood and V. Bulović, *Nano Rev.*, 2010, **1**, 5202–5208.
5 J. Tang and E. H. Sergent, *Adv. Mater.*, 2011, **23**, 12–29.
6 C.-H. M. Chuang, P. R. Brown, V. Bulovic and M. G. Bawendi, *Nat. Mater.*, 2014, **13**, 796–801.
7 F. Hetsch, N. Zhao, S. V. Kershaw and A. L. Rogach, *Mater. Today*, 2013, **16**, 312–325.
8 Landolt-Börnstein - Group III Condensed Matter, in *Group IV, Elements, IV-IV and III-V Compounds. Part b-Electronic, Transport, Optical and Other Properties*, ed. O. Madelung, U. Rössler and M. Schulz, Springer-Verlag, Germany, 2002.
9 C. Kittel, *Introduction to solid state physics*, John Wiley & Sons, Inc., USA, 8th edn, 2005.
10 W. Liu, A. Y. Chang, R. D. Schaller and D. V. Talapin, *J. Am. Chem. Soc.*, 2012, **134**, 20258–20261.
11 A. Maurice, M. L. Haro, B. Hyot and P. Reiss, *Part. Part. Syst. Charact.*, 2013, **30**, 828–831.
12 M. Yarema and M. V. Kovalenko, *Chem. Mater.*, 2013, **25**, 1788–1792.
13 R. L. Wells, C. G. Pitt, A. T. McPhail, A. P. Purdy, S. Shafieezad and R. B. Hallock, *Chem. Mater.*, 1989, **1**, 4–6.
14 O. L. Mićić, C. J. Curtis, K. M. Jones, J. R. Sprague and A. J. Nozik, *J. Phys. Chem.*, 1994, **98**, 4966–4969.
15 C. M. Evans, S. L. Castro, J. J. Worman and R. P. Raffaelle, *Chem. Mater.*, 2008, **20**, 5727–5730.
16 M. Yarema, R. Caputoa and M. V. Kovalenko, *Nanoscale*, 2013, **5**, 8398–8410.
17 K. C. Baucom and R. M. Biefeld, *Appl. Phys. Lett.*, 1994, **64**, 3021–3023.
18 H. Bürger, J. Cichon, U. Goetze, U. Wannagat and H. J. Wismar, *J. Organomet. Chem.*, 1971, **33**, 1–12.
19 H. Choi, J.-H. Ko, Y.-H. Kim and S. Jeong, *J. Am. Chem. Soc.*, 2013, **138**, 5278–5281.
20 M. Yarema, S. Pichler, D. Kriegner, J. Stangl, O. Yarema, R. Kirchschlager, S. Tollabimazraehno, M. Humer, D. Häringer, M. Kohl, G. Chen and W. Heiss, *ACS Nano*, 2012, **6**, 4113–4121.
21 G. Wu and M. Huang, *Chem. Rev.*, 2006, **106**, 2596–2616.
22 M. He, L. Protesescu, R. Caputo, F. Krumeich and M. V. Kovalenko, *Chem. Mater.*, 2015, **25**, 635–647.
23 A. H. McDaniel and M. D. Allendorf, *Chem. Mater.*, 2000, **12**, 450–460.
24 S. Salim, C. Kiang Lim and K. F. Jensen, *Chem. Mater.*, 1995, **7**, 507–516.
25 Z. Liu, A. Kumbhar, D. Xu, J. Zhang, Z. Sun and J. Fang, *Angew. Chem., Int. Ed.*, 2008, **47**, 3540–3542.
26 *Lange's Handbook of Chemistry*, ed. J. A. Dean, McGraw-Hill, New York, 15th edn, 1998.
27 X. Tangt, R. G. van Weltenis, F. M. van Setten and A. J. Bosch, *Semicond. Sci. Technol.*, 1986, **1**, 355–365.

